ATLAS CONF Note

ATLAS-CONF-2017-067

15th September 2017

Measurement of W boson production in the muon channel in Pb+Pb collisions at $\sqrt{s_{\mathrm{NN}}}$ =5.02 TeV

The ATLAS Collaboration

The production of W bosons in the muon decay channel in lead-lead collisions at a center-of-mass energy of $\sqrt{s_{\mathrm{NN}}}$ = 5.02 TeV is studied by the ATLAS experiment. The analysis is based on a data sample of 0.49 nb^{-1} collected in 2015. The dependence on centrality and muon presudorapidity of the $W \to \mu\nu$ production yields per minimum-bias event divided by the nuclear thickness function is measured for W^+ and W^- bosons within a fiducial region defined by the detector acceptance. The measured $W \to \mu\nu$ yields divided by the nuclear thickness function have no dependence on the number of participants. The lepton charge asymmetry is also measured as a function of the muon absolute pseudorapidity. The results are compared to predictions based on the next-to-next-to-leading order calculations with CT10 parton distribution functions as well as to the next-to-leading order MCFM prediction with the EPPS16 and nCTEQ15 nuclear parton distribution functions.

ATLAS-CONF-2017-067
23 September 2017

1 Introduction

Collisions between lead ions at the Large Hadron Collider (LHC) provide a way to create hot and dense strongly-interacting matter at temperatures well above the critical temperature [1]. The Relativistic Heavy Ion Collider (RHIC) established that at such temperatures, strongly interacting matter takes the form of the quark-gluon plasma (QGP) [2]. Quarks and gluons undergo interaction in the initial stages of nuclear collisions, while produced color particles are expected to lose energy interacting in the QGP, leading to the phenomenon of jet quenching [3, 4]. Both RHIC and LHC experiments reported a suppression of charged hadron yields in heavy-ion (HI) collisions [5–7].

On the other hand colorless elementary particles, which are created in hard scatterings, are transparent to the subsequent evolution of the QGP and probe the very initial stage of the collision. The PHENIX experiment at RHIC measured the properties of highly energetic photons [8], and found that their production rates scale with the nuclear thickness. In Run 1 at the LHC, both the ATLAS and CMS experiments made first measurements of electroweak vector bosons in lead-lead (Pb+Pb) collisions: isolated prompt photons [9, 10], Z and W bosons [11–13] measured in their leptonic decay modes. Their production rates were found essentially unaffected by the presence of the medium.

Weak-boson production is considered to be an important benchmark process at hadron colliders. Measurements in proton-proton (pp) collisions at $\sqrt{s}$ =7, 8 and 13 TeV at the LHC [14–17] and at previous colliders at lower energies [18–20] are well described by calculations based on higher-order perturbative quantum chromodynamics (pQCD). At leading order, W bosons are preferentially produced in $u\bar{d} \to W^+$ and $d\bar{u} \to W^-$ processes [21]. In Pb+Pb collisions due to a different quark composition of the colliding system in comparison to the pp system, the individual W^+ and W^- rates are expected to be modified, but not their sum. This is often referred to as the isospin effect, as it originates from a different content of u and d quarks in the proton relative to the lead nuclei. Furthermore, the weak boson production rates in Pb+Pb collisions may differ from that in pp collisions due to effects arising from the presence of the large nucleus where the parton distribution function (PDF) of free nucleon might be modified leading to parton depletion or enhancement [22]. The measurements of W boson production rates in HI collisions therefore provide the opportunity to extract valuable information on the nuclear modifications to the free-nucleon PDF [22, 23].

Leptonic W decays are of particular interest, since the charged leptons are expected to not interact substantially with the QGP, making them useful "penetrating" probes of the QGP. Since they are predominantly created from a left-handed quark and a right-handed anti-quark, W bosons are mostly left-handed and emitted in the quark direction, towards forward rapidities. The W^+ bosons decay to a right-handed positive lepton, which is typically produced at low values of rapidity, while the W^- bosons decay to a left-handed negative lepton which is typically produced at larger values of rapidity. The angular difference and the difference in the relative yields of W^+ and W^- bosons produced in Pb+Pb compared to pp collisions can be explored using lepton charge asymmetry, defined as the difference in differential production yields of positively and negatively charged leptons divided by their sum, as a function of the charged lepton pseudorapidity (η_ℓ):

$$A_\ell(\eta_\ell) = \frac{\mathrm{d}N_{W^+\to\ell^+\nu}/\mathrm{d}\eta_\ell - \mathrm{d}N_{W^-\to\ell^-\bar{\nu}}/\mathrm{d}\eta_\ell}{\mathrm{d}N_{W^+\to\ell^+\nu}/\mathrm{d}\eta_\ell + \mathrm{d}N_{W^-\to\ell^-\bar{\nu}}/\mathrm{d}\eta_\ell}. \quad (1)$$

In the measurement of this asymmetry as a function of η_ℓ several systematic effects cancel out in the ratio.

In nucleus-nucleus (A+A) collisions in the absence of nuclear effects, the number of events of a hard process X generally scales as follows

$$N_{\mathrm{X}} = L_{\mathrm{AA}} \cdot \sigma_{\mathrm{tot}}^{\mathrm{AA}} \cdot \langle N_{\mathrm{coll}} \rangle \frac{\sigma_{\mathrm{X}}^{pp}}{\sigma_{\mathrm{tot}}^{pp}}. \tag{2}$$

Here L_{AA} is the integrated luminosity, $\sigma_{\mathrm{tot}}^{\mathrm{AA}}$ is the total inelastic A+A cross section, $\langle N_{\mathrm{coll}} \rangle$ is the mean number of binary nucleon-nucleon collisions, σ_{X}^{pp} is the cross section for the process X in pp collisions, and $\sigma_{\mathrm{tot}}^{pp}$ is the total inelastic pp cross section. In Pb+Pb collisions at $\sqrt{s_{\mathrm{NN}}}$ = 5.02 TeV, the total inelastic Pb+Pb cross section is 7.7 b and $\langle N_{\mathrm{coll}} \rangle$ = 392 is estimated in the Glauber approach [24, 25]. The total inelastic cross section for pp collisions at the same center-of-mass energy is assumed to be 70 mb as quoted in Ref. [26]. Given that $L_{\mathrm{AA}} \times \sigma_{\mathrm{tot}}^{\mathrm{AA}}$ is the total number of inelastic events (N_{evt}), while $\langle N_{\mathrm{coll}} \rangle / \sigma_{\mathrm{tot}}^{pp}$ is the mean nuclear thickness function $\langle T_{AA} \rangle$, the measured nucleon-nucleon cross section for the process X in A+A collisions can be expressed as

$$\sigma_{\mathrm{X}}^{\mathrm{NN}} = \frac{N_{\mathrm{X}}}{N_{\mathrm{evt}} \times \langle T_{\mathrm{AA}} \rangle}. \tag{3}$$

This expression allows a direct comparison between the production yields in HI collisions normalized to give the nucleon-nucleon cross section and the pp cross section of the same hard process, either measured in pp collisions or calculated using standard MC generators. The differences between $\sigma_{\mathrm{X}}^{\mathrm{NN}}$ and σ_{X}^{pp} may arise due to nuclear effects including the isospin effect.

In this note, the first measurement of W boson production yields in the muon channel in the HI collision data at $\sqrt{s_{\mathrm{NN}}}$ = 5.02 TeV is presented. The analyzed data sample is based on Pb+Pb data collected in 2015 and corresponds to an integrated luminosity of 0.49 nb^{-1}. The lepton charge asymmetry is measured as a function of the muon absolute pseudorapidity. The results are compared to predictions based on next-to-next-to-leading order (NNLO) calculations with the use of CT10 [27] PDFs and two sets of next-to-leading order (NLO) predictions with EPPS16 [28] and nCTEQ15 [29] nuclear modifications.

2 ATLAS detector

A detailed description of the ATLAS detector is provided in Ref. [30]. The ATLAS detector consists of an inner tracking detector surrounded by a thin superconducting solenoid, electromagnetic and hadronic calorimeters and a muon spectrometer.

The inner detector (ID) provides a precise reconstruction of tracks within $|\eta| < 2.5$[1]. It consists of four layers of pixel detectors close to the beam-pipe, four layers of silicon microstrip detector modules with pairs of single-sided sensors glued back-to-back (SCT) providing eight hits per track at intermediate radii, and a transition radiation tracker (TRT) at the outer radii, providing about 35 hits per track (in the range $|\eta| < 2.0$). Before the start of Run 2, the new innermost pixel layer, the Insertable B-Layer (IBL) [31], was inserted at a mean sensor radius of 3.3 cm. A thin superconducting solenoid surrounds the ID and provides 2 T axial magnetic field.

[1] ATLAS uses a right-handed coordinate system with its origin at the nominal interaction point (IP) in the centre of the detector and the z-axis along the beam pipe. The x-axis points in the direction from the IP to the centre of the LHC ring, and the y-axis points upwards. Cylindrical coordinates (r, ϕ) are used in the transverse plane, ϕ being the azimuthal angle around the z-axis. The pseudorapidity is defined in terms of the polar angle θ as $\eta = -\ln \tan(\theta/2)$.

The calorimeter system covers the pseudorapidity range $|\eta| < 4.9$. Within the region $|\eta| < 3.2$, electromagnetic calorimetry is provided by high-granularity barrel and endcap lead/liquid-argon (LAr) electromagnetic calorimeters, with an additional thin LAr presampler covering $|\eta| < 1.8$, to correct for energy loss in material upstream of the calorimeters. Hadronic calorimetry is provided by the steel/scintilating-tile calorimeter, segmented into three barrel structures within $|\eta| < 1.7$, and two copper/LAr hadronic endcap calorimeters. Forward calorimeters (FCal) cover the range $3.1 < |\eta| < 4.9$. The FCal is a liquid-argon sampling calorimeter located on boths sides of the IP, with each half composed of one electromagnetic and two hadronic sections, with copper and tungsten serving as the absorber material, respectively.

The muon spectrometer (MS) is the outermost subdetector, designed to detect muons in the pseudorapidity region up to $|\eta| = 2.7$, and to provide momentum measurements with a relative resolution better than 3% over a wide p_{T} range and up to 10% at $p_{\mathrm{T}} \approx 1$ TeV. The MS consists of one barrel ($|\eta| < 1.05$) and two endcap sections ($1.05 < |\eta| < 2.7$). A system of three large superconducting air-core toroidal magnets, each with eight coils, provides a magnetic field with a bending integral of about 2.5 Tm in the barrel and up to 6 Tm in the endcaps. Resistive plate chambers (RPC, three doublet layers for $|\eta| < 1.05$) and thin gap chambers (TGC, one triplet layer followed by two doublet layers for $1.0 < |\eta| < 2.4$) provide triggering capability to the detector as well as (η, ϕ) position measurements with typical spatial resolution of 5-10 mm. A precise momentum measurement for muons with pseudorapidity up to $|\eta| = 2.7$ is provided by three layers of monitored drift tube chambers (MDT), with each chamber providing six to eight η measurements along the muon trajectory. For $|\eta| > 2$, the inner layer is instrumented with a quadruplet of cathode strip chambers (CSC) instead of MDTs. The single-hit resolution in the bending plane for the MDT and the CSC is about 80 μm and 60 μm, respectively. The muon chambers are aligned with a precision between 30 μm and 60 μm.

The zero-degree calorimeters (ZDC) are located symmetrically at $z = \pm 140$ m and cover $|\eta| > 8.3$. In Pb+Pb collisions the ZDC primarily measure spectator neutrons from the colliding nuclei. A ZDC coincidence trigger is implemented by requiring the summed pulse height from each ZDC to be above a threshold set below the single neutron peak.

The ATLAS detector also includes a two-level trigger system [32]: level one (L1) implemented in hardware and the software based High Level Trigger (HLT). The trigger selection for muons is performed in three steps. Information is provided to the L1 trigger system by RPCs and TGCs. At the HLT, for those events which pass L1, muon tracks are reconstructed in the vicinity of the detector region reported by the L1 trigger. A fast reconstruction of muons based on a simple algorithm which uses information from the MS, is performed and then further refined in the following step by utilizing more complex procedures as in the offline muon reconstruction software.

3 Data analysis

3.1 Data sample and trigger selection

This analysis utilizes the full set of runs with high-quality data from 2015 Pb+Pb data taking at the center-of-mass energy of $\sqrt{s_{\mathrm{NN}}} = 5.02$ TeV with integrated luminosity of 0.49 nb^{-1}.

Particle production yields in HI collisions are often presented in terms of a number of counts per minimum-bias (MB) event. The total number of MB events (N_{evt}) is extracted from a MB data sample, which

was recorded using two exclusive triggers; one designed to efficiently collect a pure sample of low-multiplicity track events and another one which selected remaining events with transverse-energy deposits above 50 GeV in the calorimeters. Both MB triggers recorded Pb+Pb data with an average suppression factor (so-called prescale) of about 20.

MB events are selected offline requiring a reconstructed primary event vertex within 150 mm along the beam line from the nominal center of the ATLAS detector. The N_{evt} parameter is evaluated as a total number of prescale-weighted MB events which were sampled during the HI run. In total, 3.74×10^9 MB collisions were sampled during the 2015 HI data-taking period.

The W boson selection requires events containing at least one muon with $p_{\text{T}} > 15$ GeV which is accepted by the HLT selection. The muon trigger efficiencies are evaluated, separately for positive and negative muons, using high-quality single muons reconstructed from MB events as well as using the Tag-and-Probe (TP) method [33] with $Z \to \mu^+\mu^-$ candidate events. Both methods give results which are in agreement within statistical uncertainties. The measured muon trigger efficiency reaches a plateau for muon $p_{\text{T}} > 15$ GeV at the level of about 70% in the barrel region and about 90% in the endcap region. The different efficiencies are due to the different geometrical acceptance of the barrel and endcap trigger systems and local detector inefficiencies.

3.2 Monte Carlo samples

Simulated Monte Carlo (MC) samples are used to calculate efficiencies and to model the properties of signal and background processes. The production of the W boson and its decays are modelled with the POWHEG-BOX v2 [34] event generator at NLO accuracy in QCD using the CT10 [27] PDF set, which is interfaced to PYTHIA 8.186 [35] in order to model parton showering and fragmentation processes. The following background processes are generated with POWHEG +PYTHIA8: $W^{\pm} \to \tau^{\pm}\nu$, $Z \to \mu^+\mu^-$, $Z \to \tau^+\tau^-$ and production of $t\bar{t}$ pairs. In addition MC samples of $c\bar{c}$ and $b\bar{b}$ events are generated using PYTHIA8 to study QCD multi-jet backgrounds. The response of the ATLAS detector is simulated using the GEANT4 framework [36].

The MC samples are produced separatelly for pp, pn, np and nn collisions and a weighting procedure is applied to combine all MC sub-samples for each sub-process of interest as described above. For each sub-process a global event weight is derived based on the mass ($A = 208$) and atomic ($Z = 82$) numbers of the colliding lead nuclei, and on the total number of generated events. This corresponds to a collision rate of $f_{pp} = (Z/A)^2 = 15.5\%$ for pp, $f_{pn} = f_{np} = Z(A-Z)/A^2 = 23.9\%$ for pn or np, and $f_{nn} = ((A-Z)/A)^2 = 36.7\%$ for nn. The global event weight for each sub-process is calculated as the ratio of the corresponding collision rate and the total number of MC events for that sub-process. In addition, W and Z boson production cross sections are scaled to NNLO accuracy using DYNNLO [37, 38] calculations with the CT14nnlo PDF set [39]. The scaling factors, denoted by k_{NNLO}, take the following values: 1.032 for W^+ boson production, 1.026 for W^- boson production and 1.007 for Z boson production. It should be noted that the k_{NNLO} factors can be calculated only for the pp isospin combination. For other isospin combinations, the same scaling as for pp collisions is assumed to be applicable.

To study detector performance in conditions that match the data, the simulated events are overlaid with events taken during the Pb+Pb run. The event data overlay is done so that the analysis of the MC simulations accurately reflects the conditions present in the Pb+Pb run. Events used in the overlay procedure were recorded using MB triggers, and with total transverse-energy triggers to enhance higher multiplicity events.

Centrality	$\langle N_{\text{part}} \rangle$		$\langle N_{\text{coll}} \rangle$		$\langle T_{\text{AA}} \rangle$ [1/mb]	
0 – 5%	384.5 ±1.9	(0.5%)	1836±130	(7.1%)	26.23±0.22	(0.84%)
5 – 10%	333.1±2.7	(0.8%)	1433±98	(6.8%)	20.47±0.20	(0.95%)
10 – 15%	285.2±2.9	(1.0%)	1126±76	(6.7%)	16.08±0.18	(1.1%)
15 – 20%	242.9±2.9	(1.2%)	881±57	(6.5%)	12.59±0.17	(1.4%)
20 – 30%	189.2±2.8	(1.5%)	605±38	(6.3%)	8.64±0.17	(2.0%)
30 – 50%	109.2±2.5	(2.3%)	265±16	(6.1%)	3.79±0.13	(3.5%)
50 – 80%	33.3±1.5	(4.5%)	48.3±3.5	(7.2%)	0.690±0.046	(6.7%)
0 – 80%	141.3±2.1	(1.5%)	490±32	(6.5%)	7.00±0.11	(1.5%)

Table 1: Parameters for different centrality classes in 2015 data. Average numbers of participating nucleons $\langle N_{\text{part}} \rangle$, binary collisions $\langle N_{\text{coll}} \rangle$, and nuclear thickness functions $\langle T_{\text{AA}} \rangle$ for each centrality class alongside with their relative uncertainties in brakets are listed.

3.3 Event centrality

In Pb+Pb collisions, the event centrality reflects the overlap volume of the two colliding nuclei. The centrality determination for the 2015 Pb+Pb data set follows similar procedures to those used for lower-energy Pb+Pb data in ATLAS and is described in Ref. [26]. The centrality of Pb+Pb events is defined using the total transverse energy measured in the FCal, evaluated at the electromagnetic scale, and denoted as FCal ΣE_{T}. Between Run 1 and Run 2, the FCal energy scale was re-calibrated because of the extra inactive material which was added to support the IBL detector. Geometric parameters and their systematic uncertainties are assigned based on the Glauber model to each centrality class by matching them to the FCal ΣE_{T} distribution. Nuclear geometry and the pp cross section are input parameters to the model as discussed in Ref. [40, 41]. The uncertainties on the model-dependent parameters originate from two main sources: (1) the uncertainties of the Glauber model itself, such as measured parameters of the Woods-Saxon distribution, the pp cross section, etc., and (2) the uncertainties of the mapping of the model onto the FCal ΣE_{T} distribution. The analysis uses seven centrality intervals: 0-5% (largest FCal ΣE_{T} values and degree of nuclear overlap), 5-10%, 10-15%, 15-20%, 20-30%, 30-50%, and 50-80% (smallest FCal ΣE_{T} values and degree of nuclear overlap). Table 1 lists the main centrality parameters with their uncertainties relevant to this analysis: the number of participating nucleons in both colliding lead nuclei ($\langle N_{\text{part}} \rangle$), the number of binary collisions ($\langle N_{\text{coll}} \rangle$), and the nuclear thickness function ($\langle T_{\text{AA}} \rangle$).

In order to improve the MC modelling of the ΣE_{T} distribution in the FCal detector in simulation, the simulated events are re-weighted to match the data.

3.4 Muon identification

Muons are reconstructed and identified following the procedures used by the ATLAS Collaboration in pp collisions at $\sqrt{s} = 13$ TeV as described in Ref. [33]. The analysis requires one muon reconstructed based on track segments recorded by the various MS layers which are matched with ID tracks resulting in a combined muon candidate. The TRT was operated during the 2015 Pb+Pb run using Argon instead of Xenon gas, leading to a strong centrality dependence of muon reconstruction performance. Thus, the TRT is not utilized in this analysis.

In the offline analysis, the p_{T} requirement and identification criteria for muons are made more stringent with respect to those applied in the trigger in order to reduce the contribution from background processes. The analysis is further restricted to the muon p_{T} region where the trigger efficiency is high and stable.

The background from muons originating from heavy-flavour decays is reduced by requiring muons to be isolated. Several isolation criteria are considered in this analysis. Their optimization is performed as a function of centrality using the TMVA tool [42]. The optimal variable is found to be the sum of transverse momenta of tracks in the cone of the size $\Delta R = \sqrt{(\Delta\eta)^2 + (\Delta\phi)^2} = 0.2$ around a muon candidate divided by muon p_{T}. The isolation requirement is varied as a function of centrality to maintain a 90% efficiency of the signal selection.

The TP method is used in order to compare muon reconstruction and identification performance in data and MC simulation. It utilizes a selected sample of $Z \to \mu^+\mu^-$ events in the 2015 Pb+Pb data which amounts to about 5000 candidates. Differences between muon performance in the data and MC simulation are accounted for by the so-called "scale factors", defined as the ratio of muon identification efficiencies in data and simulation. They are found to differ from unity by no more than 3% for $|\eta_\mu| < 1.5$, and up to 8% for $|\eta_\mu| > 1.5$. No differences in scale factors between positive and negative muons are found. Scale factors are applied as weights to the simulated events.

3.5 Missing transverse momentum and transverse mass

Neutrinos escape detection and their presence in the event is inferred from missing transverse momentum in the detector. In HI collisions, low-p_{T} particle production is significantly enhanced compared to pp collisions, thereby resulting in an increased number of particles that do not reach the calorimeters. Consequently, the resolution of missing transverse momentum defined using calorimeter cells in the data is much worse, and at the level of 45 GeV in the most central HI events [12]. Therefore, tracks are used instead of calorimeter cells, and the missing momentum vector $p_{\mathrm{T}}^{\mathrm{miss}}$ is defined as the negative vector sum of the ID track transverse momenta, except for the muon where the MS reconstructed p_{T}^{μ} is used. This approach is analogous to the one developed in pp collisions [43]. In order to further optimise background rejection and preserve a sufficient number of tracks in the vector summation, only tracks with $p_{\mathrm{T}} > 4$ GeV are used in the calculation of $p_{\mathrm{T}}^{\mathrm{miss}}$.

At the detector level, the transverse mass of the muon and neutrino system is defined as:

$$m_{\mathrm{T}} = \sqrt{2 p_{\mathrm{T}}^{\mu} p_{\mathrm{T}}^{\mathrm{miss}} (1 - \cos\Delta\phi)} \tag{4}$$

where $\Delta\phi$ is the difference between the direction of the muon and the $p_{\mathrm{T}}^{\mathrm{miss}}$ vector in the azimuthal plane.

3.6 W boson selection

W boson candidates in the $W \to \mu\nu$ decay channel are selected by:

$$p_{\mathrm{T}}^{\mu} > 25\,\mathrm{GeV}, \qquad 0.1 < |\eta_\mu| < 2.4, \qquad p_{\mathrm{T}}^{\mathrm{miss}} > 25\,\mathrm{GeV}, \qquad m_{\mathrm{T}} > 40\,\mathrm{GeV}$$

The range of η_μ reflects the coverage of the MS chambers and the acceptance of the muon trigger system. The $p_{\mathrm{T}}^{\mathrm{miss}}$ requirement contributes to the selection of a pure sample of $W \to \mu\nu$ events. The requirement on m_{T} is imposed to further reduce background events that satisfy the p_{T}^{μ} and $p_{\mathrm{T}}^{\mathrm{miss}}$ criteria.

The background contribution from $Z \to \mu^+\mu^-$ decays is further suppressed by imposing a Z-veto requirement. Events with at least two muons which form an opposite-charge pair with the invariant mass greater than 66 GeV are rejected. These events are selected by requiring that one muon in the pair has $p_{\mathrm{T}}^{\mu} > 25$ GeV and fullfiles all other quality criteria discussed in Section 3.4 and the other muon in the pair satisfies a lower p_{T} threshold of 20 GeV with the loose quality requirements.

After imposing all W boson selection criteria, 25245 candidate events with positive muons and 23123 candidate events with negative muons are selected for further analysis.

3.7 Background estimation

Jet production via QCD processes (referred to as "QCD multi-jet background") is a dominant background contribution of this analysis. It has significant components from semi-leptonic decays of heavy quarks and from muons coming from in-flight particle decays. Muons originating from these processes will generally be non-isolated, as compared to signal muons. Nevertheless, a small fraction of muons from the QCD multi-jet process fulfils the muon isolation requirement and contributes to the signal.

The QCD multi-jet background is evaluated using a data-driven approach similar to the one utilized in W boson measurements in pp collisions [44, 45]. To extract shapes of muon η_μ and p_{T}^{μ} distributions for these background events, a jet-enriched region is defined by selecting muons that fulfil the W boson requirements, except for the isolation criterion which is replaced by a set of anti-isolation requirements. Several slices of width of 0.2 in the muon isolation variable starting just above the nominal muon isolation value are studied. The contribution from W boson signal as well as Z and $W \to \tau\nu$ boson backgrounds to the jet-enriched region is subtracted. For each anti-isolation slice and centrality range, muon η_μ and p_{T}^{μ} distributions are extracted. The anti-isolation requirements in these jet-enriched samples are designed to be progressively closer to the isolation requirement defining the signal sample. The muon η_μ and p_{T}^{μ} distributions in the jet-enriched samples are then used to estimate the shapes of these distributions for QCD multi-jet events contributing to the signal sample. A set of shape correction factors is used to extrapolate these distributions from jet-enriched samples to the signal sample.

The normalization of QCD multi-jet background is extracted from a fit of the extrapolated muon p_{T} distribution to the data in the range $20 < p_{\mathrm{T}} < 50$ GeV assuming contributions from signal, electroweak backgrounds, and $t\bar{t}$ production. An alternative data-driven approach utilizes a fit in a control region defined using the nominal analysis requirements, except for the cut on muon p_{T}, which is required to be in the range $15 < p_{\mathrm{T}} < 20$ GeV. The extrapolated distributions of non-isolated muons are subsequently normalized to the number of isolated muons in the control region after the subtraction of signal and other background contributions. The number of QCD multi-jet events in the signal region is evaluated by integrating the p_{T} spectrum of non-isolated muons for $p_{\mathrm{T}} > 25$ GeV after the above-mentioned normalization procedure.

The contributions from the QCD multi-jet background for positive and negative muons are estimated separately for all centrality classes. They vary from 6% to 12%.

The electroweak background processes considered in this analysis include $W \to \tau\nu$ events with muons arising from tau decays, as well as $Z \to \mu^+\mu^-$ events, where one lepton from the Z boson decay is emitted outside the detector acceptance and produces a spuriously-large value of $p_{\mathrm{T}}^{\mathrm{miss}}$. Their contributions to the W boson candidate sample are 1.8% and 3.2%, respectively. Other possible sources of electroweak background, such as $Z \to \tau^+\tau^-$ where at least one τ decays into a muon, and $t\bar{t}$ events in which at least

one top quark decays semileptonically into a muon, contribute to below < 0.5%. The above electroweak backgrounds are estimated using POWHEG MC samples assuming cross sections for the generated processes scaled by the k_{NNLO} factors.

An additional source of background may arise in the MC overlay sample from signal muons in MB events that are used in the overlay procedure. Those muon candidates are called overlay muons. Such a background could bias muon distributions in the MC simulation and might affect the MC efficiency correction procedure. Therefore, to study a potential contribution of overlay muons to the MC samples, the analysis is performed using a pure MB sample in data. After imposing all W boson selection criteria, 49 events are identified which constitute 0.003% of the total MB sample. Therefore, this background is considered to be negligible in the analysis.

In Fig. 1 p_{T}^{μ} distributions in data and the estimated signal and background processes, after the complete set of selection requirements, are shown separately for positive and negative muons in the 0 – 80% centrality range. Error bars represent statistical uncertainties on the data points. The sum of signal and background processes describes the data to within 5% both in shape and normalization.

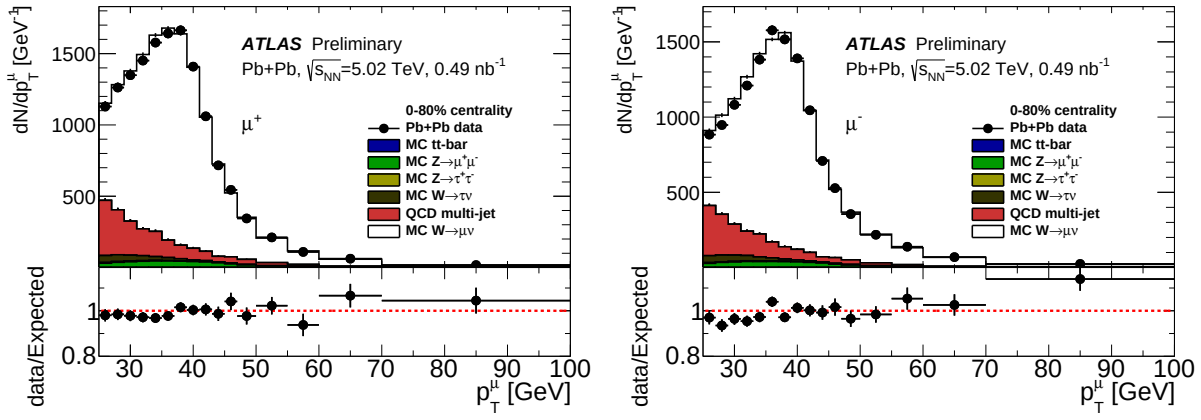

Figure 1: Transverse-momentum distributions for muons selected as candidates from W^+ (left) and W^- (right) decays after the $W \to \mu\nu$ selection is imposed in the 0 – 80% centrality range. The electroweak and $t\bar{t}$ backgrounds are taken from MC predictions while the QCD multi-jet one from the data-driven procedure as described in the text. Error bars on the data points reflect statistical uncertainties.

3.8 Signal yield extraction

The W boson production yields in the $W \to \mu\nu$ decay channel are measured in a fiducial region defined by:

$$p_{\mathrm{T}}^{\mu} > 25\,\mathrm{GeV}, \qquad 0.1 < |\eta_{\mu}| < 2.4, \qquad p_{\mathrm{T}}^{\nu} > 25\,\mathrm{GeV}, \qquad m_{\mathrm{T}} > 40\,\mathrm{GeV}$$

where p_{T}^{ν} stands for the neutrino p_{T}, and m_{T} denotes the transverse mass of the muon and neutrino system. The $W \to \mu\nu$ event yields are extracted in each pseudorapidity and centrality bin using the formula:

$$N_{W^{\pm}} = \frac{N_{W^{\pm}}^{\mathrm{obs}} - N_{W^{\pm}}^{\mathrm{bkg}}}{C_W}, \tag{5}$$

where $N_{W^\pm}^{\text{obs}}$ and $N_{W^\pm}^{\text{bkg}}$ are the numbers of observed and background events and C_W is a bin-by-bin correction factor calculated using the signal $W \to \mu\nu$ MC sample and defined as follows:

$$C_W(\eta_\mu^{\text{reco}}, \text{centrality}) = \frac{N_W^{\text{sel,pass}}(\eta_\mu^{\text{reco}}, \text{centrality})}{N_W^{\text{sel,gen}}(\eta_\mu^{\text{true}}, \text{centrality})}, \tag{6}$$

with $N_W^{\text{sel,pass}}$ being the number of muon candidates that fulfil the W boson selection criteria at the detector level, as discussed in previous sections, in the given eta (η_μ^{reco}) and centrality bin, while $N_W^{\text{sel,gen}}$ denotes the number of muons from W boson decays selected in the fiducial phase space defined at generator level as functions of the muon pseudorapidity (η_μ^{true}) and centrality.

The C_W factors correct for muon reconstruction and identification efficiencies, resolution and QED radiation effects. They also account for the inefficiency due to the Z-veto requirement. They are derived separately for μ^+ and μ^- as a function of muon η_μ and event centrality. Integrating over η_μ, the total C_W amounts to approximately 70% for μ^+ and 73% for μ^- in the 0 – 80% centrality range.

4 Systematic uncertainties

Systematic uncertainties are determined separately for each muon charge, pseudorapidity bin and event centrality class. Several sources of systematic uncertainties are considered in the analysis:

- One of the most significant systematic uncertainties originates from the muon trigger efficiency. The precision of that correction is limited by the number of $Z \to \mu^+\mu^-$ events available in the 2015 Pb+Pb sample and utilized in the TP method. Therefore, the statistical uncertainty is considered as a measure of the systematic uncertainties, and its impact on the signal yield is evaluated by varying the trigger efficiency up and down in a correlated way between bins. The impact on the W boson yields as a function of η_μ is around 3%.
- Another systematic uncertainty is associated with the selection of the threshold on the track p_{T} in the calculation of $p_{\text{T}}^{\text{miss}}$. The uncertainty is estimated by varying the nominal threshold of 4 GeV by ±1 GeV. The size of the resulting uncertainty is at the level of 2%.
- The nominal muon isolation requirement is optimised to obtain 90% signal efficiency. For determination of the systematic uncertainty due to muon isolation, the 85% and 95% signal efficiency working points are utilised. This results in an average variation of 2% for W boson yields as a function of η_μ.
- The contribution from the QCD multi-jet background is evaluated as the difference in results obtained using two data-driven approaches described in Section 3.7. For the nominal measurement, the result from the fit in $20 < p_{\text{T}} < 50$ GeV is used, while the control-region method is applied for evaluation of the systematic uncertainty. This alternative approach leads to differences in the W boson yields as a function of η_μ which typically are between 3% and 5%. They are largest in the central η_μ region where this background contribution is the most significant. These differences are assigned as systematic uncertainties.
- To estimate the systematic uncertainty due to the electroweak and $t\bar{t}$ backgrounds the nominal cross sections are varied by ±5% and ±6% [15], respectively. Using a conservative assumption, the normalizations of the W and Z production rates are taken to be fully correlated. The resulting uncertainty on the signal yield originating from the electroweak background varies between 0.2% and 0.5% and

Source	Average uncertainty [%]	Uncertainty range [%]
Muon trigger efficiency	3.3	1.6 – 6.2
$p_{\mathrm{T}}^{\mathrm{miss}}$ reconstruction	1.1	0 – 4.4
Muon isolation	1.0	0.1 – 5.5
QCD multi-jet background	5.0	2.0 – 7.2
Muon efficiency	1.2	0.7 – 2.3
Track momentum scale	1.0	0.04 – 1.9
Electroweak backgrounds	0.3	0.2 – 0.6
$t\bar{t}$ background	0.01	0 – 0.02
Muon p_{T} resolution	< 0.01	-
Total	7.1	2.8 – 9.1

Table 2: Ranges and average values of the relative systematic uncertainties in percentages on the measured signal yields as a function of the muon η_μ in the 0 – 80% centrality range.

is comparable for both muon charges. The systematic uncertainty associated with the $t\bar{t}$ production is found to contribute less than 0.1% of the signal yield.

- In order to estimate the uncertainties originating from differences in the muon reconstruction and identification efficiencies between data and MC simulation, the scale factors discussed in Section 3.4 are varied by their statistical uncertainties. Conservatively, it is done in a correlated way between all bins. The impact on the yields as a function of the muon η_μ is around 1.5%.
- The systematic uncertainty due to the muon p_{T}^{μ} resolution is evaluated by applying an additional smearing to the p_{T}^{μ} distribution in MC simulation. The resulting uncertainty on the W boson yields is found to be below 0.1% and as such it is considered negligible in the analysis.
- An additional uncertainty takes into account a possible residual misalignment of the tracking detectors in the Pb+Pb data. The track momentum scale is varied by ±2% in the data. The impact on the signal yields as a function of η_μ is around 1% and almost constant over the entire η_μ range.
- The $\langle T_{\mathrm{AA}} \rangle$ parameter is utilised to normalize the W boson production yields. The uncertainties on $\langle T_{\mathrm{AA}} \rangle$ are given in Table 1 and they amount to up to 1.4% for 0-20% centralities and grow to almost 7% for the 50-80% centrality bin. That uncertainty is propagated to the final results by varying the data normalization factors up and down by this value. The impact on the W boson yields as a function of the muon η_μ is around 1.5% constant over the entire η_μ range.

For each individual systematic source the upward and downward deviations from the nominal value are evaluated. The total systematic uncertainty is the sum in quadrature of all individual contributions. Table 2 summarizes all sources of systematic uncertainties and their contributions to systematics on the W boson yields as a function of the muon η_μ in the 0-80% centrality range. In the lepton charge asymmetry, uncertainties on the normalization from $\langle T_{\mathrm{AA}} \rangle$ cancel out. Similarly, the uncertainties originating from the electroweak and $t\bar{t}$ backgrounds largely cancel.

5 Results

The total numbers of background-subtracted and efficiency-corrected events for the process $W \to \mu\nu$ in the fiducial region are 34500 ± 290 (stat.) $^{+2100}_{-2600}$ (syst.) and 31300 ± 270 (stat.) $^{+1900}_{-2500}$ (syst.) in the W^+

and W^- boson samples, respectively.

Figure 2 shows the W boson production yields in the fiducial region per MB event divided by $\langle T_{\rm AA}\rangle$ as a function of $\langle N_{\rm part}\rangle$ separately for W^+ and W^- bosons. Yields of W bosons divided by $\langle T_{\rm AA}\rangle$ are observed to be independent of centrality. Moreover, $W^+ \to \mu^+\nu$ yields are systematically about 10% larger than $W^- \to \mu^-\bar{\nu}$ yields. The data is compared to POWHEG predictions scaled by the $k_{\rm NNLO}$ factor using CT10 free-nucleon PDF and a good agreement is found.

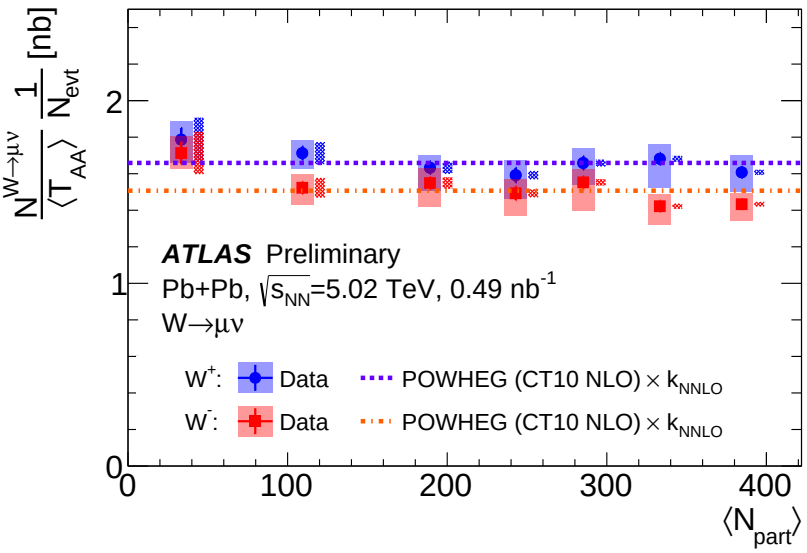

Figure 2: Fiducial $W \to \mu\nu$ yields per MB event divided by $\langle T_{\rm AA}\rangle$ as a function of $\langle N_{\rm part}\rangle$ for W^+ and W^- for $p_{\rm T}^{\mu} > 25$ GeV, $p_{\rm T}^{\nu} > 25$ GeV, $m_{\rm T} > 40$ GeV and $0.1 < |\eta_{\mu}| < 2.4$. Error bars represent statistical uncertainties. Systematic and statistical uncertainties added in quadrature are shown as the filled boxes around data points while the systematic uncertainties related to the $\langle T_{\rm AA}\rangle$ are presented by the hatched area shifted along the x-axis for better visibility. MC statistical uncertainties are negligible.

Figure 3 shows the differential production yields per MB event divided by $\langle T_{\rm AA}\rangle$ as a function of η_{μ} separately for W^+ and W^- bosons extracted from the 0 – 80% centrality range. The distribution for W^+ is approximately constant for $|\eta_{\mu}| < 1$ and then falls at larger η_{μ} values, whereas for W^- only a small η dependence is observed. The data is compared to POWHEG predictions scaled by the $k_{\rm NNLO}$ factor using CT10 free-nucleon PDF. The MC expectations are consistent with the data. Two predictions based on MCFM [46], a parton-level MC program that calculates cross sections to NLO accuracy in QCD for a range of processes at hadron colliders, using the most recent nuclear modifications to PDF, EPPS16 [28] and nCTEQ15 [29], are also shown. They both underestimate the data, however a 2-3% difference between the NNLO-scaled POWHEG and MCFM predictions is expected due to the different order of the QCD calculations, i.e. the contribution of the NNLO radiative effects. The remaining difference is consistent with observations reported in Ref. [23].

Figure 4 shows a comparison of differential W boson production yields as a function of the lepton absolute pseudorapidity $|\eta_{\ell}|$ measured in Pb+Pb collisions at two center-of-mass energies 2.76 [12] and 5.02 TeV along with the POWHEG predictions. The 2.76 TeV measurement combines data from muon and electron decay channels. The W boson yields grow with collision energy as expected. Shapes of the differential

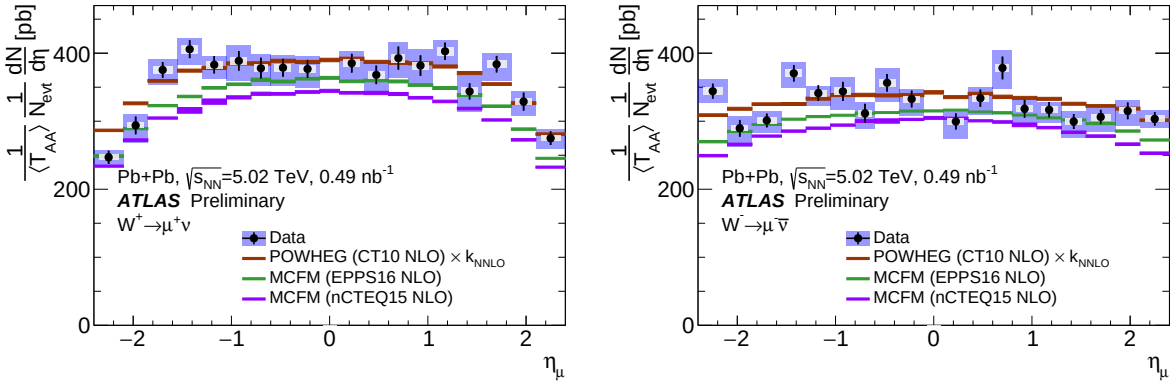

Figure 3: Differential production yields per MB event divided by $\langle T_{\mathrm{AA}} \rangle$ for $W^+ \to \mu^+ \nu$ (left) and $W^- \to \mu^- \bar{\nu}$ (right) extracted from the 0 – 80% centrality range as a function of pseudorapidity for $p_{\mathrm{T}}^{\mu} > 25$ GeV, $p_{\mathrm{T}}^{\nu} > 25$ GeV, $m_{\mathrm{T}} > 40$ GeV. The measured distributions are compared to POWHEG scaled by k_{NNLO} with CT10 PDF, and to MCFM NLO predictions with EPPS16 and nCTEQ15 nPDF. Error bars represent statistical uncertainties. Systematic and statistical uncertainties added in quadrature are shown as the filled boxes, while the systematic uncertainties related to $\langle T_{\mathrm{AA}} \rangle$ are presented by the white boxes. The width of the theory bands reflects MC statistical uncertainties.

yields are similar between the two energies. The statistical precision of the 5.02 TeV measurement is a factor of two better than the Run-1 result. The CT10 POWHEG predictions agree well with the data.

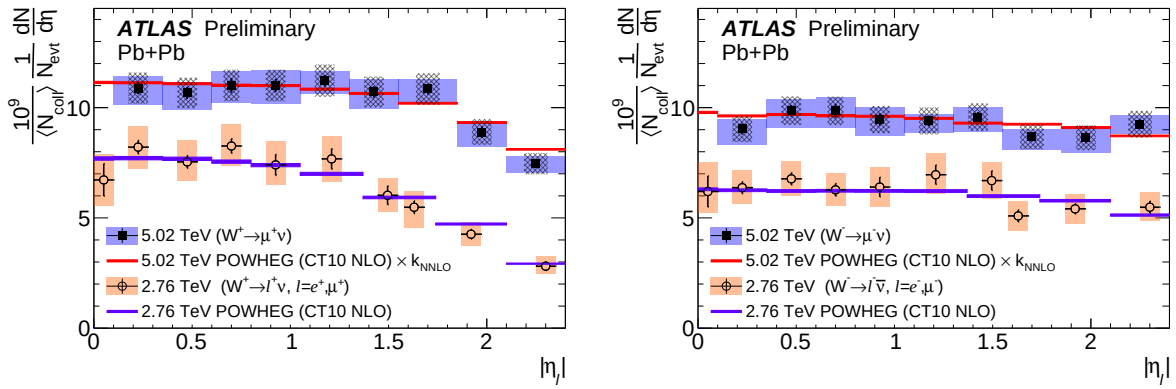

Figure 4: Differential production yields per binary collision ($\langle N_{\mathrm{coll}} \rangle$) and per MB event ($N_{\mathrm{evt}}$) for $W^+ \to \ell^+ \nu$ (left) and $W^- \to \ell^- \bar{\nu}$ (right) extracted from the 0 – 80% centrality range as a function of absolute value of pseudorapidity for $p_{\mathrm{T}}^{\ell} > 25$ GeV, $p_{\mathrm{T}}^{\nu} > 25$ GeV, $m_{\mathrm{T}} > 40$ GeV. The measured distributions are compared to the Run 1 results [12] at 2.76 TeV. For the 5.02 TeV results only the muon decay channel is shown ($\ell = \mu$), whereas for the 2.76 TeV results a combination of electron and muon channels is shown ($\ell = e, \mu$). POWHEG predictions with CT10 PDF are shown for both energies. The 5.02 TeV POWHEG NLO prediction is scaled by the k_{NNLO} factor. Error bars represent statistical uncertainties. Systematic and statistical uncertainties added in quadrature are shown as the filled boxes, while the systematic uncertainties related to the $\langle N_{\mathrm{coll}} \rangle$ for the 5.02 TeV data points are presented by the hatched boxes. The width of the theory bands reflects MC statistical uncertainties.

Figure 5 shows the lepton charge asymmetry defined in Eq. 1 and extracted from the 0 – 80% centrality range as a function of the muon absolute pseudorapidity. The muon charge asymmetry is roughly constant at the level of 6% in $|\eta_\mu| < 1.4$ and then decreases with increasing $|\eta_\mu|$. It becomes negative for $|\eta_\mu| > 2$.

Predictions from POWHEG scaled by k_{NNLO} using the CT10 PDF set and NLO MCFM with two nuclear PDFs, i.e. EPPS16 and nCTEQ15, are shown. The predictions describe the data well in $|\eta_\mu| < 1.4$. For higher $|\eta_\mu|$ values the data points deviate by no more than 3σ from the theory.

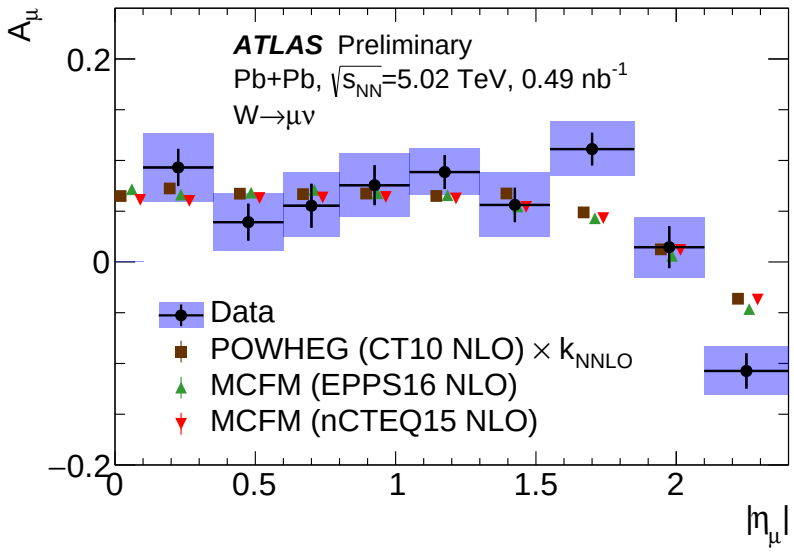

Figure 5: Muon charge asymmetry for $W \to \mu\nu$ events extracted from the 0 – 80% centrality range as a function of absolute pseudorapidity. Theory predictions are indicated with the markers shifted along the x-axis for better visibility. Error bars represent statistical uncertainties, whereas systematic uncertainties added in quadrature are shown as the filled boxes. Systematics related to $\langle T_{\mathrm{AA}} \rangle$ cancel out in the ratio. The MC statistical uncertainties are smaller than the size of markers.

6 Summary

In this analysis, $W \to \mu\nu$ yields are measured in Pb+Pb collisions at $\sqrt{s_{\mathrm{NN}}} = 5.02$ TeV with an integrated luminosity of 0.49 nb^{-1} by the ATLAS detector at the LHC. The $W^{\pm}$ boson candidates decaying into the muon channel are selected in the fiducial region defined by $p_{\mathrm{T}}^{\mu} > 25$ GeV, $0.1 < |\eta_\mu| < 2.4$, $p_{\mathrm{T}}^{\nu} > 25$ GeV and $m_{\mathrm{T}} > 40$ GeV.

The $W \to \mu\nu$ yields divided by the number of minimum-bias events and by the nuclear thickness function are presented as a function of η_μ and $\langle N_{\mathrm{part}} \rangle$. The W boson yields integrated over η_μ are found to scale with $\langle T_{\mathrm{AA}} \rangle$ in all centrality ranges. The $W^+ \to \mu^+\nu$ yields are found to be about 10% larger compared to the $W^- \to \mu^-\bar{\nu}$ yields and in agreement with the POWHEG prediction using CT10 parton distribution functions and corrected for the NNLO inclusive production cross section. Differential yields in η_μ are in agreement with the NNLO-scaled POWHEG. The MCFM calculations using EPPS16 and nCTEQ15 PDF sets underestimate the data. The muon charge asymmetry is roughly constant at the level of 6% in $|\eta_\mu| < 1.4$ and then decreases for higher $|\eta_\mu|$ values. It is in good agreement with all three predictions for $|\eta_\mu| < 1.4$. For higher $|\eta_\mu|$ values there are discrepancies between the data and predictions.

References

[1] A. Andronic and P. Braun-Munzinger,
Ultrarelativistic nucleus-nucleus collisions and the quark gluon plasma,
Lect. Notes Phys. **652** (2004) 35, arXiv: hep-ph/0402291 [hep-ph].

[2] PHENIX Collaboration, *Formation of dense partonic matter in relativistic nucleus-nucleus collisions at RHIC: Experimental evaluation by the PHENIX collaboration*,
Nucl. Phys. **A 757** (2005) 184, arXiv: nucl-ex/0410003 [nucl-ex].

[3] Y. Mehtar-Tani, J. G. Milhano and K. Tywoniuk, *Jet physics in heavy-ion collisions*,
Int. J. Mod. Phys. **A 28** (2013) 1340013, arXiv: 1302.2579 [hep-ph].

[4] G.-Y. Qin and X.-N. Wang, *Jet quenching in high-energy heavy-ion collisions*,
Int. J. Mod. Phys. **E 24** (2015) 1530014, [,309(2016)], arXiv: 1511.00790 [hep-ph].

[5] PHENIX Collaboration,
High p_T charged hadron suppression in Au + Au collisions at $\sqrt{s_{NN}}$ = 200 GeV,
Phys. Rev. **C 69** (2004) 034910, arXiv: nucl-ex/0308006 [nucl-ex].

[6] ATLAS Collaboration, *Measurement of charged-particle spectra in Pb+Pb collisions at $\sqrt{s_{\rm NN}}$ = 2.76 TeV with the ATLAS detector at the LHC*, JHEP **09** (2015) 050,
arXiv: 1504.04337 [hep-ex].

[7] CMS Collaboration, *Study of high-p_T charged particle suppression in PbPb compared to pp collisions at $\sqrt{s_{NN}}$ = 2.76 TeV*, Eur. Phys. J. **C 72** (2012) 1945, arXiv: 1202.2554 [nucl-ex].

[8] PHENIX Collaboration,
Measurement of Direct Photons in Au+Au Collisions at $\sqrt{s_{NN}}$ = 200 GeV,
Phys. Rev. Lett. **109** (2012) 152302, arXiv: 1205.5759 [nucl-ex].

[9] ATLAS Collaboration,
Centrality, rapidity and transverse momentum dependence of isolated prompt photon production in lead-lead collisions at $\sqrt{s_{\rm NN}}$ = 2.76 TeV measured with the ATLAS detector,
Phys. Rev. **C 93** (2016) 034914, arXiv: 1506.08552 [hep-ex].

[10] CMS Collaboration,
Measurement of isolated photon production in pp and PbPb collisions at $\sqrt{s_{NN}}$ = 2.76 TeV,
Phys. Lett. **B 710** (2012) 256, arXiv: 1201.3093 [nucl-ex].

[11] ATLAS Collaboration, *Measurement of Z boson Production in Pb+Pb Collisions at $\sqrt{s_{NN}}$ = 2.76 TeV with the ATLAS Detector*, Phys. Rev. Lett. **110** (2013) 022301,
arXiv: 1210.6486 [hep-ex].

[12] ATLAS Collaboration, *Measurement of the production and lepton charge asymmetry of W bosons in Pb+Pb collisions at $\sqrt{s_{\rm NN}}$=2.76 TeV with the ATLAS detector*, Eur. Phys. J. **C 75** (2015) 23,
arXiv: 1408.4674 [hep-ex].

[13] CMS Collaboration,
Study of W boson production in PbPb and pp collisions at $\sqrt{s_{NN}}$ = 2.76 TeV,
Phys. Lett. **B 715** (2012) 66, arXiv: 1205.6334 [nucl-ex].

[14] ATLAS Collaboration, *Measurement of the $W \to \ell\nu$ and $Z/\gamma^* \to \ell\ell$ production cross sections in proton-proton collisions at $\sqrt{s}$ = 7 TeV with the ATLAS detector*, JHEP **12** (2010) 060,
arXiv: 1010.2130 [hep-ex].

[15] ATLAS Collaboration, *Measurement of $W^{\pm}$ and Z-boson production cross sections in pp collisions at $\sqrt{s}$ = 13 TeV with the ATLAS detector*, Phys. Lett. **B 759** (2016) 601, arXiv: 1603.09222 [hep-ex].

[16] CMS Collaboration, *Measurement of the Inclusive W and Z Production Cross Sections in pp Collisions at $\sqrt{s}$ = 7 TeV*, JHEP **10** (2011) 132, arXiv: 1107.4789 [hep-ex].

[17] CMS Collaboration, *Measurement of inclusive W and Z boson production cross sections in pp collisions at $\sqrt{s}$ = 8 TeV*, Phys. Rev. Lett. **112** (2014) 191802, arXiv: 1402.0923 [hep-ex].

[18] SLD Electroweak Group, DELPHI, ALEPH, SLD, SLD Heavy Flavour Group, OPAL, LEP Electroweak Working Group, L3, S. Schael et al., *Precision electroweak measurements on the Z resonance*, Phys. Rept. **427** (2006) 257, arXiv: hep-ex/0509008 [hep-ex].

[19] CDF Collaboration, *Measurements of inclusive W and Z cross sections in p anti-p collisions at s**(1/2) = 1.96-TeV*, J. Phys. **G 34** (2007) 2457, arXiv: hep-ex/0508029 [hep-ex].

[20] D0 Collaboration, *Measurement of the W Boson Production Charge Asymmetry in $p\bar{p} \to W + X \to e\nu + X$ Events at $\sqrt{s}$ = 1.96 TeV*, Phys. Rev. Lett. **112** (2014) 151803, [Erratum: Phys. Rev. Lett.114,no.4,049901(2015)], arXiv: 1312.2895 [hep-ex].

[21] A. D. Martin, R. G. Roberts, W. J. Stirling and R. S. Thorne, *Parton distributions and the LHC: W and Z production*, Eur. Phys. J. **C 14** (2000) 133, arXiv: hep-ph/9907231 [hep-ph].

[22] R. Vogt, *Shadowing effects on vector boson production*, Phys. Rev. **C 64** (2001) 044901, arXiv: hep-ph/0011242 [hep-ph].

[23] H. Paukkunen and C. A. Salgado, *Constraints for the nuclear parton distributions from Z and W production at the LHC*, JHEP **03** (2011) 071, arXiv: 1010.5392 [hep-ph].

[24] B. Alver, M. Baker, C. Loizides and P. Steinberg, *The PHOBOS Glauber Monte Carlo*, (2008), arXiv: 0805.4411 [nucl-ex].

[25] M. L. Miller, K. Reygers, S. J. Sanders and P. Steinberg, *Glauber modeling in high energy nuclear collisions*, Ann. Rev. Nucl. Part. Sci. **57** (2007) 205, arXiv: nucl-ex/0701025 [nucl-ex].

[26] ATLAS Collaboration, *Study of photon-jet momentum correlations in Pb+Pb and pp collisions at $\sqrt{s_{\mathrm{NN}}}$ = 5.02 TeV with ATLAS*, (2016), URL: https://cds.cern.ch/record/2220772.

[27] H.-L. Lai et al., *New parton distributions for collider physics*, Phys. Rev. **D 82** (2010) 074024, arXiv: 1007.2241 [hep-ph].

[28] K. J. Eskola, P. Paakkinen, H. Paukkunen and C. A. Salgado, *EPPS16: Nuclear parton distributions with LHC data*, Eur. Phys. J. **C 77** (2017) 163, arXiv: 1612.05741 [hep-ph].

[29] K. Kovarik et al., *nCTEQ15 - Global analysis of nuclear parton distributions with uncertainties in the CTEQ framework*, Phys. Rev. **D 93** (2016) 085037, arXiv: 1509.00792 [hep-ph].

[30] ATLAS Collaboration, *The ATLAS Experiment at the CERN Large Hadron Collider*, JINST **3** (2008) S08003.

[31] M Capeans et al., *ATLAS Insertable B-Layer Technical Design Report*, ATLAS-TDR-19, (2010), URL: https://cds.cern.ch/record/1291633.

[32] ATLAS Collaboration, *Performance of the ATLAS Trigger System in 2015*, Eur. Phys. J. **C 77** (2017) 317, arXiv: 1611.09661 [hep-ex].

[33] ATLAS Collaboration, *Muon reconstruction performance of the ATLAS detector in proton–proton collision data at $\sqrt{s}$ =13 TeV*, Eur. Phys. J. **C 76** (2016) 292, arXiv: 1603.05598 [hep-ex].

[34] S. Alioli, P. Nason, C. Oleari and E. Re, *A general framework for implementing NLO calculations in shower Monte Carlo programs: the POWHEG BOX*, JHEP **06** (2010) 043, arXiv: 1002.2581 [hep-ph].

[35] T. Sjostrand, S. Mrenna and P. Z. Skands, *A Brief Introduction to PYTHIA 8.1*, Comput. Phys. Commun. **178** (2008) 852, arXiv: 0710.3820 [hep-ph].

[36] S. Agostinelli et al., *GEANT4: A Simulation toolkit*, Nucl. Instrum. Meth. **A 506** (2003) 250.

[37] S. Catani and M. Grazzini, *An NNLO subtraction formalism in hadron collisions and its application to Higgs boson production at the LHC*, Phys. Rev. Lett. **98** (2007) 222002, arXiv: hep-ph/0703012 [hep-ph].

[38] S. Catani, L. Cieri, G. Ferrera, D. Florian and M. Grazzini, *Vector boson production at hadron colliders: a fully exclusive QCD calculation at NNLO*, Phys. Rev. Lett. **103** (2009) 082001, arXiv: 0903.2120 [hep-ph].

[39] S. Dulat et al., *New parton distribution functions from a global analysis of quantum chromodynamics*, Phys. Rev. **D 93** (2016) 033006, arXiv: 1506.07443 [hep-ph].

[40] B. Alver, M. Baker, C. Loizides and P. Steinberg, *The PHOBOS Glauber Monte Carlo*, (2008), arXiv: 0805.4411 [nucl-ex].

[41] M.L. Miller, K. Reygers, S.J. Sanders and P. Steinberg, *Glauber Modeling in High Energy Nuclear Collisions*, Ann. Rev. Nucl. Part. Sci. **57** (2007) 205.

[42] A. Hoecker et al., *TMVA: Toolkit for Multivariate Data Analysis*, PoS **ACAT** (2007) 040, arXiv: physics/0703039.

[43] ATLAS Collaboration, *Measurement of the missing transverse momentum based on tracks in proton-proton collisions at $\sqrt{s} = 900$ GeV centre-of-mass energy with the ATLAS detector*, ATLAS-CONF-2010-020, (2010), URL: https://cds.cern.ch/record/1277652.

[44] ATLAS Collaboration, *Measurement of the W-boson mass in pp collisions at $\sqrt{s} = 7$ TeV with the ATLAS detector*, (2017), arXiv: 1701.07240 [hep-ex].

[45] ATLAS Collaboration, *Precision measurement and interpretation of inclusive W^+ , W^- and Z/γ^* production cross sections with the ATLAS detector*, Eur. Phys. J. **C77** (2017) 367, arXiv: 1612.03016 [hep-ex].

[46] J. M. Campbell, R. K. Ellis and W. T. Giele, *A Multi-Threaded Version of MCFM*, Eur. Phys. J. **C 75** (2015) 246, arXiv: 1503.06182 [physics.comp-ph].